"Partial-Coupled Mode-Space" A new Approach for Efficient Simulation of Ballistic Quantum Transport in Multi-gate Devices

Mohammed M. El-Banna, Yasser M. Sabry, W. Fikry, O. A. Omar

Dept. of Eng. Physics and Mathematics, Faculty of Engineering, Ain Shams University, Egypt.
mm.elbanna@eng.asu.edu.eg

Abstract: A novel approach is proposed, termed Partial-Coupled Mode Space (PCMS), for simulation of quantum transport in nanoscale devices. The PCMS integrates advantage of Coupled Mode Space (CMS) in accuracy and Uncoupled Mode Space (UMS) in reduction of computational burden. Partial coupling between the modes of the nanoscale device is achieved by coupling the odd-modes and even-modes separately. N-type FinFETs were simulated by the proposed approach and compared with the fully CMS accuracy and simulation time. The simulation was carried out on set of devices that satisfy the requirements of the International Technology Roadmap for Semiconductors (ITRS). The simulations show that our PCMS saves more than 65 % of the computational time with error less than 0.1 % and 0.01 % in the device charge and terminal current respectively compared to the CMS.
[Mohammed M. El-Banna, Yasser M. Sabry, W. Fikry, O. A. Omar. **"Partial-Coupled Mode-Space" A new Approach for Efficient Simulation of Ballistic Quantum Transport in Multi-gate Devices** *J Am Sci* 2013;9(3):329-338]. (ISSN: 1545-1003). http://www.jofamericanscience.org. 57

Keywords: FinFETs, Partial-Coupled Mode Space, Multi-gate, quantum transport, NEGF.

1. Introduction

The development of new structures has been one of the most important achievements in device engineering to overcome scaling of bulk MOSFETs transistors to the nanoscale era [1]. FinFETs and nanowire MOSFETs are strongly considered for generations of silicon-integrated devices that satisfy the requirements of the International Technology Roadmap for Semiconductors (ITRS) [2]. Quantum mechanical effects (QME) play a crucial role in device performance and parameters [3]. Therefore, accurate and efficient device simulation tools are necessary to interpret experimental results, and to provide device and process design guidelines for the fabrication of such structures.

Among the new simulation methods, Non-equilibrium Green's function Formalism (NEGF) shows a strong potential for modeling nanoscale devices where ballistic or inelastic scattering transport simulation dominate [4]. Device simulation is carried out using the so-called self-consistent solution within the NEGF framework [5]. Iterations are carried out between Poisson's and quantum transport's equations until a solution satisfying both are achieved within a certain tolerance. This makes the simulation speed very challenging in addition to the complexity of the NEGF, therefore, computational efficient methods are needed.

Within NEGF, Real-Space (RS) representation is the most accurate approach. Consuming time is the main obstacle for its usage in device simulation due to the huge size of the Hamiltonian matrix of the device region for two or three dimensional calculations. In order to accelerate RS calculations, efforts have been exerted by using different techniques [5,6] but the computational efficiency is still not satisfactory and investigations of alternative approaches to the accurate RS approach were needed. Recently, mode space (MS) approach has been proposed [7,8] in which the wave functions are expanded in terms of the device eigen functions. As a result, the transport calculation can be simplified to a one-dimensional problem along the transport direction [9]. The Uncoupled-Mode Space (UMS) is the fastest approach ignoring the coupling between all the device's modes and treating the transport problem of each mode separately [10,11]. Within the MS approach, the Schrödinger equation is calculated either on every slice perpendicular to the transport direction or on one slice only [12] or an analytical approximation is used [13] to further reduce the computations but sacrificing the simulations accuracy. Unfortunately, the limitation to ultra thin devices only (5 nm thick or less) constrained the usage of UMS approach [9,10]. The Coupled-Mode Space (CMS) fully accounts for the coupling terms between the modes resulting in more accurate simulation [12,14] in which the CMS computational burden is in between the RS and the UMS. Ben Abdallah *et al.* [15] proposed the modeling of ballistic quantum transport in nanostructures using the decomposition of the wave function which reduced simulation time. A. Paussa et al. [16] presented the possible advantages related to the use of the Pseudospectral (PS) method for the efficient description of the carrier quantization in nanoscale n- and p-MOS transistors. An efficient carbon nanotube (CNT) transistor modeling technique that is based on cubic spline approximation of the non-equilibrium

mobile charge density has been reported [17]. Artificial neural network (ANN) for modeling and simulation of carbon nanotube metal–oxide-semiconductor field-effect transistors (CNT-MOSFETs) have been applied in [18]. In [19], a three dimensional (3D) numerical modeling of nanoscale FinFET including quantum-mechanical effects has been developed. The exact potential profile in the channel has been computed by obtaining a self-consistent solution of 3D Poisson–Schrödinger equation using Leibmann's iteration method. In [20], a quantum transport model using wavelet method based on the self-consistent solution of 3-D Poisson-Schrödinger equation has been reported using multi-resolution approach. Efficient schemes for the non-equilibrium Green's function simulation in the mode space formalism of electron-phonon scattering using the self-consistent Born approximation in nanoscale devices have been developed [21]. The existing literatures reported on analytical and numerical modeling have shown the complexity in evaluating various device characteristics including QME. In addition, it has been found that many assumptions and approximations have to be incorporated while the device is modeled.

In this work, we propose a novel approach for solving the NEGF within the MS representation. By incorporating partial coupling between the modes, the proposed approach takes the advantage of CMS in accuracy and UMS in the efficiency. As a case study, the N-channel FinFET is taken but the approach can be, in principle, applied to other structures such as CNT, nanowires and multigate devices. The proposed model as well as the CMS approache was implemented into the FETMOSS simulator [22]. When the new approach is benchmarked with the CMS, it shows very good performance as for accuracy, memory requirements and CPU time. In this paper, we first describe the device structure and briefly review the CMS approach theory in section 2. In section 3, calculation of the coupling terms on sample devices from the ITRS is carried out and the proposed PCMS is introduced. In section 4, results on the simulation time and accuracy of the PCMS with respect to the CMS are presented and discussed. Finally, the article is concluded in section 5.

2. Finfet Structure and Coupled-Mode Space Aproach

Figure 1 (a) shows the FinFET device considered in this study. The top gate oxide thickness was assumed to be much thicker than the side gate oxide such that channels are formed under the side gate oxides only. Consequently, the simulation domain was assumed to be 2D as shown in Figure 1 (b). The following assumptions are valid for FETMOSS simulator as in the literature:

1) Channel length (*x*-direction) is shorter than any characteristic scattering length, so the device is operating in the ballistic limit [23].
2) The width (in the *z*-direction) is large compared to its length and thickness [10].
3) Large drain and source contacts, so the Fermi level is determined by the applied voltage [4].
4) Zero gate current during the self-consistent solution due to the isolation of the insulator region from electron penetration [10].
5) N-channel transistor where we can neglect holes contribution.
6) Finally, a single band effective mass Hamiltonian is used to model the electron transport with parabolic *E-K* relation [3].

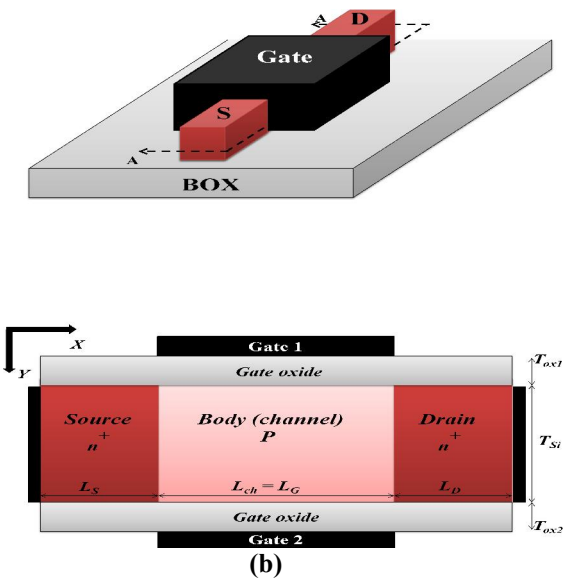

(b)

Figure 1. (a) 3-D view of a FinFET, (b) A-A cross-section

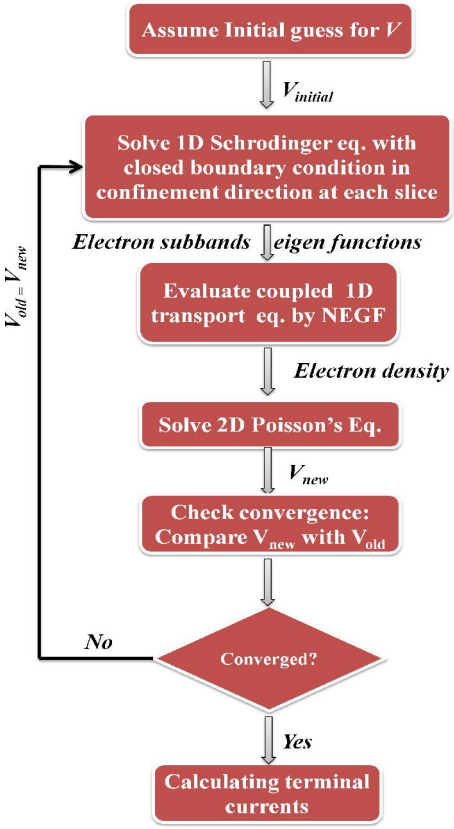

Figure 2. Flow chart of simulation of Coupled-Mode space approach in 2D simulation.

The flow chart shown in Figure 2 illustrate the procedure of calculating CMS approach as follows: First, initial guess was assumed by running ballistic transport model using semi-classical approach in FETMOSS simulator [22] for one iteration. Second, a one dimensional (1D) Schrödinger equation with a closed boundary condition was solved at each slice (vertical *y*-direction) of the transistor to obtain the electron subbands (along the transistor) and the corresponding eigenfunctions. Third, coupled 1D transport equation was solved by NEGF approach [3,4] for the electron charge density. Fourth, the two dimensional (2D) Poisson's equation for the electrostatic potential was solved. Finally, the new potential was compared with the old one. If it converges, then the electron current by the NEGF approach was calculated. Otherwise, second, third and fourth steps were continued.

In MS representation, the envelope wave function $\psi(x, y, z)$ is expanded in terms of the ortho-normal basis $[\psi(x,y)\exp(jk_Z)]/\sqrt{w}$ where the quantum number K_Z corresponds to the transverse eignenergy $E_{K_Z} = \hbar^2 K_Z^2/2m_Z^*$, m_Z^* is the electron effective mass in the *z*-direction and w is the channel width. From solving the 2D Schrödinger equation:

$$\left[-\frac{\hbar^2}{2m^*_x}\frac{\partial^2}{\partial x^2} - \frac{\hbar^2}{2m^*_y}\frac{\partial^2}{\partial y^2} + E_C(x,y)\right]\psi(x,y) = \left(E - E_{k_z}\right)\psi(x,y) = E_l\psi(x,y) \quad (1)$$

the 2D wave function $\psi(x, y)$ is obtained, where m_x^* and m_y^* are the electron effective mass in *x*- and *y*-direction respectively, E_C is the conduction band edge, E is the total energy, and E_l is the longitudinal energy due to motion in *x*- and *y*- plane. By choosing suitable expansion for 2D wave function $\psi(x,y)$ [24], a coupled 1D Schrödinger equation is obtained [25]:

$$-\frac{\hbar^2}{2m^*_x}\frac{\partial^2\phi^{(m)}(x)}{\partial x^2} + [E^{(m)}(x) - E_l]\phi^{(m)}(x) = \sum_{n=1}^{n=N_m}[a_{mn}(x) + b_{mn}(x)]\phi^{(n)}(x) \quad (2)$$

where $$a_{mn}(x) = -\frac{\hbar^2}{2m^*_x}\left[\int dy \chi^{*(m)}(x,y)\frac{\partial^2}{\partial x^2}\chi^{(n)}(x,y)\right]$$

and $$b_{mn}(x) = -\frac{\hbar^2}{2m^*_x}\left[2\int dy \chi^{*(m)}(x,y)\frac{\partial}{\partial x}\chi^{(n)}(x,y)\right]$$

$\phi^{(m)}(x)$ are the expansion coefficients, $\chi^{(n)}(x, y)$ are the modes associated with confinement in the (transverse) *y*-direction, $E^{(m)}(x)$ represents the bottom of the mode m and N_m is maximum number of subbands (modes). For each mth mode, the right hand side of eq. (2) involves a summation over all other modes including the m^{th} mode itself. This summation gives rise to coupling between the modes. Only a few of the lowest modes (i.e., $m, n = 1,...,N_m$, $N_m < N_y$) are occupied and need to be included in the simulation, due to quantum confinement. Eq. (3) implies a set of N_m equations that is in the matrix form:

$$[H_{CMS}]\{\phi^{(m)}\} = [E_l I]\{\phi^{(m)}\}$$

where
$$[H_{CMS}] = \begin{bmatrix} h_{11} & h_{12} & h_{13} & \cdots & h_{1N_m} \\ h_{21} & h_{22} & h_{23} & \cdots & h_{2N_m} \\ h_{31} & h_{32} & h_{33} & \cdots & h_{3N_m} \\ \vdots & \vdots & \vdots & \vdots & \vdots \\ h_{N_m 1} & h_{N_m 2} & h_{N_m 3} & \cdots & h_{N_m N_m} \end{bmatrix}_{N_m x N_m} , \{\phi^{(m)}\} = \begin{Bmatrix} \phi^1(x) \\ \phi^2(x) \\ \phi^3(x) \\ \vdots \\ \phi^{N_m}(x) \end{Bmatrix}_{N_m x 1} \quad (3)$$

and
$$h_{mn}(x) = [-\frac{\hbar^2}{2m^*_x}\frac{\partial^2}{\partial x^2} + E_m(x)]\delta_{m,n} - a_{mn}(x) - b_{mn}(x)\frac{\partial}{\partial x} \quad (4)$$

where h_{mn} matrix dimension is (N_x x N_x), N_x is the number of grid points in x-direction and δ_{mn} is the Kronecker delta function.

Finally, the NEGF framework calculates the electron density and current after the device Hamiltonian is obtained [4,12,26,27]. The CMS fully account for the different terms of eq. (2) while the UMS completely ignores the right hand side of this equation and set to zero. In the next section, we show that only partial coupling between the modes is needed, for accurate simulation, depending on whether the mode shape (or index) is odd or even.

3. Proposed Partial-Coupled Mode Space

The PCMS approach has the advantage of accuracy with reduction of simulation time with respect to CMS approach. This reduction depend on two criteria: The first one is the criteria of choosing the suitable number of modes that contains charge density which contributes in the charge and current calculations. The second one is the criteria of eliminating some coupling terms between modes that have no contribution in calculating charge and current.

The coupling effect of the mth mode on the nth mode is defined by the coupling term that was stated in eq. (2).

$$C_{mn}(E_l, x) = [a_{mn}(x) + b_{mn}(x)]\phi^{(n)}(x; E_l) \quad (5)$$

It depends on both the longitudinal energy and the x-position along the transistor channel. Coupling terms are used as indicator of whether the coupling between the modes is important or can be neglected. The simulator FETMOSS [5,11,22] was modified to calculate these terms for assessing their importance hereinafter.

For this study, we select five devices to cover the ITRS targets from the year 2013 up to the year 2021[2]. Table 1 lists the parameters of these devices. All devices were subjected to PCMS and CMS simulation. When we go through showing results graphically, we will concentrate on device 3 to avoid repeating results. The transistor channel is intrinsic and the gate metal work function is 4.65eV. For source and drain regions, doping was selected to be $2x10^{20}cm^{-3}$ while length was 5nm.

Table 1Device parameters list used in simulation

Device	1	2	3	4	5
Year of production	2013	2015	2017	2019	2021
Channel length L (nm)	13	10	8	6	5
Si thickness T_{Si} (nm)	7.5	6	4.5	3.8	3.2
SiO_2 thickness T_{ox} (nm)	0.6	0.6	0.55	0.5	0.5
Supply voltage V_{DD} (V)	0.9	0.8	0.7	0.7	0.65

Quantum confinement creates steps in the energy from one mode to the higher order one and so few modes are only needed. When the energy becomes too high, the mode is almost not occupied by electrons and has negligible effect on the simulation results. Thus, a criteria for determining the suitable number of modes is needed. After several iterations, we found that taking modes with charge density $\geq 10^{-3}$ of the lowest order mode's charge density is sufficient for charge and current calculations. An example is shown in Figure 3 where device 3 is simulated and the 2D charge density for different modes is depicted. The needed number of modes in this case is 4. By using

the same criteria, the numbers of modes are 7, 6, 4 and 3 for devices 1, 2, 4 and 5 respectively. The use of larger number of modes will increase the simulation time without adding value to the accuracy.

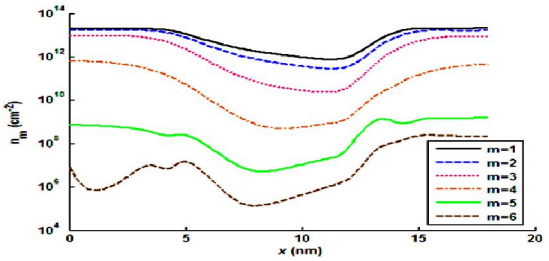

Figure 3. 2D electron density of different modes along the channel in *x*-direction for device 3 in on-state

To determine the eliminated coupling terms according to the second criteria, we will consider the maximum absolute values of the coupling terms $|C_{mn}|_{max}$. The value of these quantities was studied at different bias conditions and only on-state ($V_{GS} = V_{DS} = V_{DD}$) and off-state ($V_{GS} = 0V$ and $V_{DS} = V_{DD}$) are enough for demonstrating our results. The same observations of these two cases were found for other different bias conditions.

$|C_{mn}|_{max}$ is calculated and presented in Table 2 (a) and (b) for device 1 in off- and on-states respectively. The common observation among all modes is that there is (are) always one or two dominant term(s) where the other terms are order of magnitude smaller and can be neglected. For example, $C_{13}|_{max}$ is the dominate term for the 1st order mode, $C_{24}|_{max}$ for the 2nd order mode, $C_{31}|_{max}$ and $C_{35}|_{max}$ for the 3rd order mode and so on….. Table 3 (a) and (b) (Table 4 (a) and (b)) list the quantity $|C_{mn}|_{max}$ for device 2 (device 3) in off- and on-states respectively, where similar results were obtained. In fact the same observation was found for all other devices under study.

Table 2

(a) $|C_{mn}|_{max}$ for device 1 in off-state with dominant terms highlighted

m / n	1	2	3	4	5	6	7
1	0.02	0.05	0.51	0.02	0.06	0.01	0.01
2	0.05	0.04	0.03	0.70	0.01	0.08	0.00
3	0.5	0.03	0.06	0.02	0.7	0.01	0.09
4	0.01	0.67	0.02	0.07	0.01	0.65	0.00
5	0.06	0.01	0.70	0.01	0.07	0.01	0.55
6	0.00	0.09	0.01	0.65	0.01	0.06	0.01
7	0.01	0.00	0.09	0.00	0.60	0.01	0.06

(b) $|C_{mn}|_{max}$ for device 1 in on-state with dominant terms highlighted

	1	2	3	4	5	6	7
1	0.01	0.07	0.31	0.02	0.05	0.01	0.01
2	0.07	0.01	0.02	0.36	0.01	0.01	0.00
3	0.33	0.02	0.02	0.03	0.33	0.01	0.06
4	0.02	0.35	0.03	0.02	0.01	0.26	0.00
5	0.05	0.01	0.34	0.01	0.02	0.01	0.23
6	0.01	0.07	0.01	0.30	0.01	0.02	0.01
7	0.02	0.00	0.07	0.00	0.26	0.01	0.01

Table 3

(a) $|C_{mn}|_{max}$ for device 2 in off-state with dominant terms highlighted

m / n	1	2	3	4	5	6
1	0.01	0.03	0.43	0.01	0.04	0.00
2	0.03	0.02	0.02	0.48	0.01	0.05
3	0.41	0.01	0.03	0.01	0.44	0.00
4	0.01	0.50	0.01	0.04	0.01	0.39
5	0.05	0.01	0.46	0.01	0.03	0.01
6	0.00	0.05	0.00	0.39	0.01	0.03

(b) $|C_{mn}|_{max}$ for device 2 in on-state with dominant terms highlighted

m / n	1	2	3	4	5	6
1	0.01	0.04	0.25	0.01	0.04	0.00
2	0.04	0.01	0.01	0.26	0.00	0.04
3	0.27	0.01	0.01	0.01	0.23	0.00
4	0.01	0.26	0.01	0.01	0.00	0.18
5	0.04	0.01	0.23	0.01	0.01	0.00
6	0.01	0.04	0.00	0.20	0.00	0.01

Table 4

(a) $|C_{mn}|_{max}$ for device 3 in off-state with dominant terms highlighted

m / n	1	2	3	4
1	0.01	0.01	0.26	0.00
2	0.01	0.01	0.01	0.23
3	0.26	0.01	0.01	0.00
4	0.00	0.26	0.00	0.01

(b) $|C_{mn}|_{max}$ for device 3 in on-state with dominant terms highlighted

m / n	1	2	3	4
1	0.00	0.01	0.16	0.00
2	0.08	0.00	0.01	0.15
3	0.19	0.01	0.01	0.00
4	0.00	0.16	0.00	0.00

One can create asymmetry in the energy band structure if there is difference in the gates oxide thickness or if the applied voltages for both gates are not the same [28]. Table 5 (a) presents the quantity

$|C_{mn}|_{max}$ for device 2 in off-state as the structure is asymmetric. The front gate oxide thickness = 0.6nm and the back gate oxide thickness = 0.2nm for the structure in Figure 1. The observation is that for each mode, there are always more than two dominant term(s). For example, $C_{12}|_{max}$, $C_{13}|_{max}$, $C_{14}|_{max}$ and $C_{15}|_{max}$ are the dominate terms for the 1st order mode, $C_{21}|_{max}$, $C_{23}|_{max}$, $C_{24}|_{max}$, $C_{25}|_{max}$ and $C_{26}|_{max}$ for the 2nd order mode and so on. This observation is common for any other different dimensions in gate oxide thickness. Table 5 (b) presents the quantity $|C_{mn}|_{max}$ for device 2 in on-state as the structure is asymmetric where the front gate voltage = 0.8V and the back gate voltage = 0.4V. The observation is that for each mode, there are always two or more dominant term(s) as in the previous case. This observation is common for any other asymmetric applied voltage on the two gates. We can conclude that neglection of the coupling between some modes is valid only in case of symmetric structure with symmetric applied voltage for both gates.

Table 5

(a) $|C_{mn}|_{max}$ for device 2 in off-state with dominant terms highlighted for asymmetric dimensions: front gate oxide thickness = 0.6nm and back gate oxide thickness = 0.2nm

n \ m	1	2	3	4	5	6
1	0.01	0.50	0.31	0.16	0.12	0.09
2	0.52	0.02	0.61	0.38	0.22	0.17
3	0.32	0.64	0.03	0.73	0.40	0.27
4	0.15	0.40	0.78	0.04	0.85	0.46
5	0.12	0.22	0.41	0.91	0.06	0.96
6	0.09	0.17	0.27	0.47	1.04	0.07

(b) $|C_{mn}|_{max}$ for device 2 in on-state with dominant terms highlighted for asymmetric voltages: front gate voltage = 0.8V and back gate voltage = 0.4V

n \ m	1	2	3	4	5	6
1	0.01	0.25	0.28	0.02	0.04	0.01
2	0.27	0.03	0.30	0.30	0.02	0.04
3	0.30	0.32	0.04	0.33	0.28	0.02
4	0.02	0.32	0.33	0.04	0.28	0.22
5	0.04	0.02	0.28	0.30	0.03	0.23
6	0.01	0.05	0.02	0.25	0.25	0.025

The existence of few dominant terms among the coupling terms in symmetric FinFET structure indicates that no need for full coupling among the modes (which is the CMS). We can notice that the problem can be decoupled into two smaller problems, for device 1 as an example, where modes number 2, 4 and 6 have to be solved together due to their significant coupling. At the same time, modes number 1, 3, 5 and 7 follow the same case. Therefore, we have one problem in three unknowns and the other one in four unknowns. Generally, the problem with N_m unknowns can be divided into two smaller problems; one for the odd modes and the other one for the even modes. The size of these problems is $N_m/2$ and $N_m/2$, if N_m is even or $(N_m-1)/2$ and $(N_m+1)/2$, if N_m is odd. Since the solution of a linear system of N unknowns involves N^3 operations [29], the proposed PCMS relative operations count with respect to the CMS is:

$$N_{rel} = 2(N_m/2)^3 / N_m^3 = 25\% \text{ , if } N_m \text{ is even} \qquad (6)$$
$$N_{rel} = \{[(N_m-1)/2]^3 + [(N_m+1)/2]^3\} / N_m^3 \text{ , if } N_m \text{ is odd}$$

In the language of the NEGF, the PCMS means we divide the Hamiltonian matrix in eq. (3) into two separate Hamiltonians H_{odd} and H_{even} that are given by:

$$H_{odd} = \begin{bmatrix} h_{11} & h_{13} & h_{15} & \cdots & h_{1i} \\ h_{31} & h_{33} & h_{35} & \cdots & h_{3i} \\ h_{51} & h_{53} & h_{55} & \cdots & h_{5i} \\ \vdots & \vdots & \vdots & \ddots & \vdots \\ h_{i1} & \cdots & \cdots & \cdots & h_{ii} \end{bmatrix}_{p \times p}, \quad H_{even} = \begin{bmatrix} h_{22} & h_{24} & h_{26} & \cdots & h_{2j} \\ h_{42} & h_{44} & h_{46} & \cdots & h_{4j} \\ h_{62} & h_{64} & h_{66} & \cdots & h_{6j} \\ \vdots & \vdots & \vdots & \ddots & \vdots \\ h_{j2} & \cdots & \cdots & \cdots & h_{jj} \end{bmatrix}_{q \times q} \qquad (7)$$

where $i = N_m - 1$, $j = N_m$, $p = N_m/2$ and $q = N_m/2$, if N_m is an even number; while $i = N_m$, $p = (N_m+1)/2$, $j = (N_m-1)$ and $q = (N_m-1)/2$, if N_m is an odd number. Terms connecting even and odd modes are all neglected. The electron density and terminal current can be then calculated normally within the NEGF [4] but one time for the odd modes and a second time for the even modes and their contributions are added.

4. RESULTS AND DISCUSSION

The proposed PCMS approach as well as the CMS approach were implemented and integrated in the FETMOSS simulator [22]. A study was carried out on the devices given in Table 1. The purpose of this study is to check the accuracy of the PCMS with respect to the CMS and to compare the practical reduction in simulation time with eq. (6). The simulation was carried out on a home PC with 3GHz, Core 2 Quad 64 bit AMD processor and 8GB RAM memory.

The solution of Schrödinger equation in the transverse direction (y -direction) in Figure 1 results in subband energies whose values vary in the channel direction. Figure 4 depicts well matching of the profiles of subband edges along the channel (x-direction) for device 3 in on-state for the four lowest subbands in the primed valley using PCMS and CMS approaches. The four subbands are chosen according to the first criteria mentioned before in section 3.

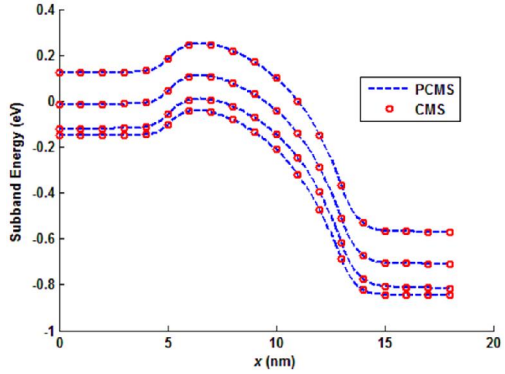

Figure 4. Subband energy profile along the channel for device 3 in on-state for the four lowest subbands in the primed valley using PCMS and CMS approaches

The occupation of the different subbands with carriers is calculated from the 2D subband carrier density N_{2D} (cm^{-2}). Figure 5 illustrates the *2D* electron density of the lowest subbands along the channel for device 3 in on-state. In comparing PCMS with respect to CMS approaches, the maximum percentage error equal 0.2% with 72.6 % reduction in simulation time according to second criteria.

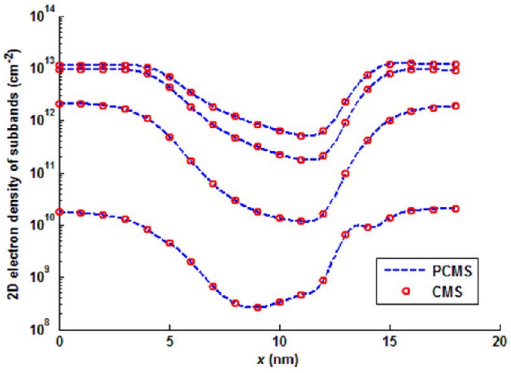

Figure 5. 2D electron density of the lowest four subbands along the channel for the primed valley for device 3 in on-state using PCMS and CMS approaches.

Figure 6 and Figure 7 show the 3D distribution of the potential energy and electron concentration simulated for device 3 in on-state respectively. The error in results between PCMS and CMS approaches is less than 0.002 % and 0.02 % respectively according to the first criteria.

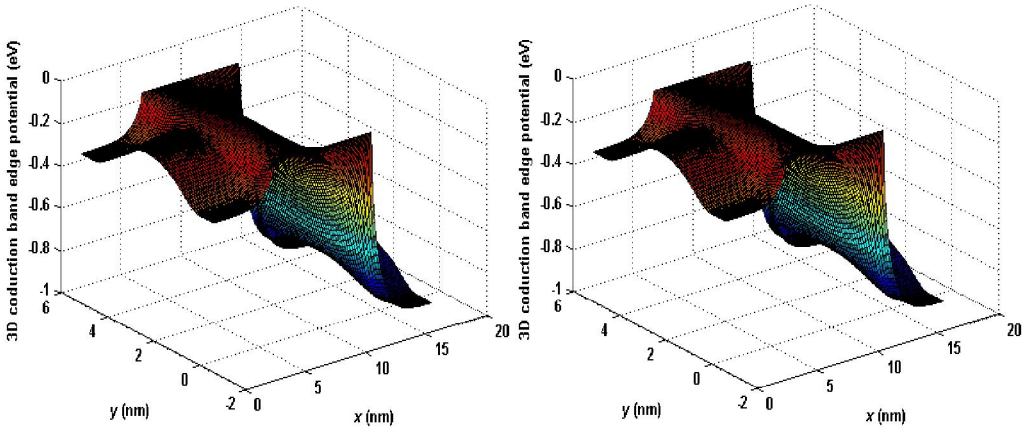

(a) **(b)**

Figure 6. The *3D* distribution of the potential energy for device 3 in on-state for both (a) PCMS and (b) CMS approaches.

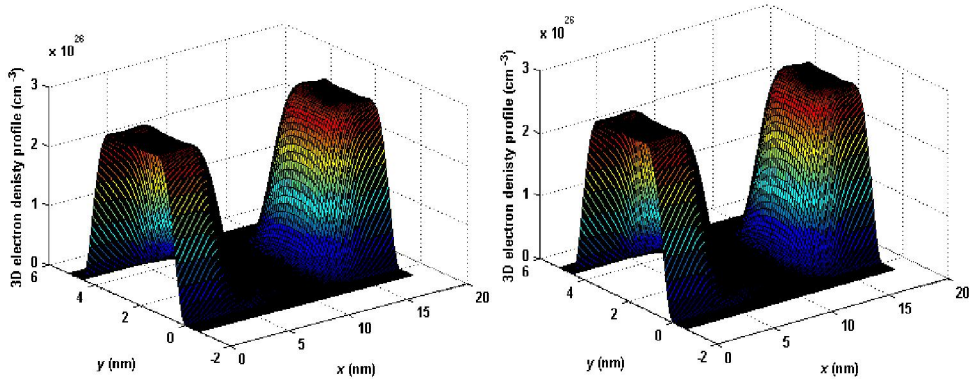

Figure 7. The *3D* distribution of electron concentration simulated for device 3 in on-state for both (a) PCMS and (b) CMS approaches.

The transmission coefficient and terminal current versus energy for device 3 in on-state are demonstrated in Figure 8 and Figure 9 respectively. There is an excellent agreement between the results of the proposed PCMS and the CMS approaches for both transmission coefficient and terminal current with 72.6 % computational burden reduction by satisfying second criteria.

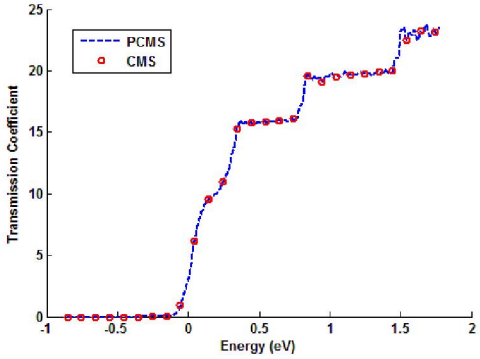

Figure 8. The transmission coefficient versus energy for device 3 in on-state using PCMS and CMS approaches.

.

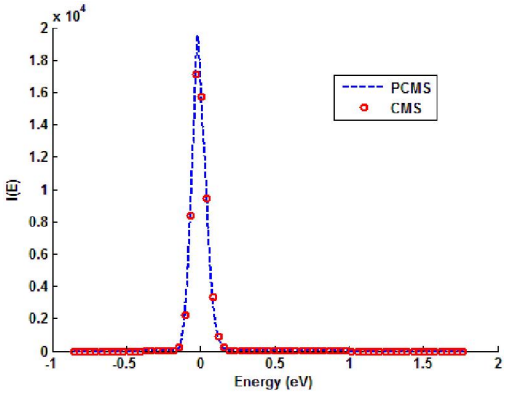

Figure 9. The terminal current versus energy for device 3 in on-state using PCMS and CMS approaches

Figure 10 illustrates a sample I_{DS} -V_{DS} characteristics at different V_{GS} for device 3. The drain voltage was swept from 0 to V_{DD} (0.7V) with steps of 0.1V while the gate voltage was swept from 0.3 to 0.7V in steps of 0.1V.

According to the first criteria, the curves predict exactitude results between the proposed PCMS and the CMS approaches.

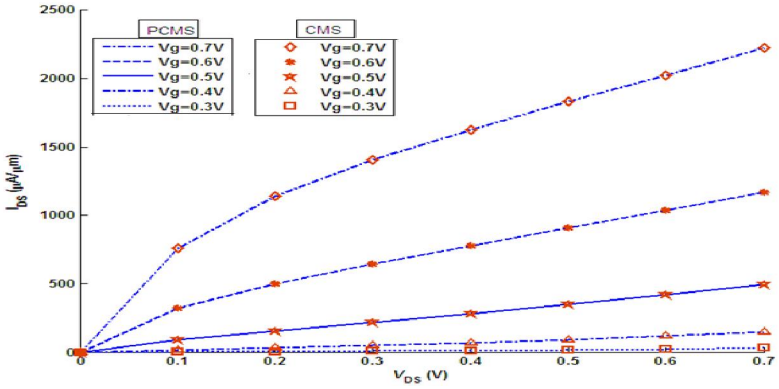

Figure 10. I_{DS}-V_{DS} family of curves for device 3 at different V_{GS} using PCMS and CMS approaches.

The percentage difference in terminal current and electron charge density (3D distribution) between PCMS and CMS were calculated and tabulated in Table 6 for the various simulated devices. They are defined as:

$$\Delta I = \left|\frac{I_{CMS} - I_{PCMS}}{I_{CMS}}\right| x100, \quad \Delta n = \max\left|\frac{n_{CMS} - n_{PCMS}}{n_{CMS}}\right| x100 \qquad (8)$$

The simulation was repeated many times for different bias conditions to check the relative accuracy of PCMS. Excellent agreement was found between the PCMS and the CMS in all bias conditions and for all the simulated devices. Among these bias conditions, the cases of off- and on-states are given in Table 6.

Table 6
Accuracy and computations reduction of the PCMS relative to CMS

Device	1	2	3	4	5
N_m	7	6	4	4	3
Δn off-state	7×10^{-1}	5×10^{-1}	1×10^{-1}	2×10^{-3}	3×10^{-3}
Δn on-state	1×10^{-1}	3×10^{-2}	2×10^{-2}	2×10^{-3}	2×10^{-3}
ΔI off-state	6×10^{-3}	9×10^{-4}	3×10^{-5}	10×10^{-4}	3×10^{-4}
ΔI on-state	1×10^{-2}	5×10^{-3}	3×10^{-5}	2×10^{-4}	3×10^{-5}
N_{rel}	27.2	25	25	25	33.3
t_{rel} off-state	26.8	28.6	27.6	26.5	34.9
t_{rel} on-state	26.9	26.1	27.4	26.4	35.1

We define the relative time taken by the PCMS simulation and the CMS simulation by:

$$t_{rel} = \frac{t_{PCMS}}{t_{CMS}} x100 \qquad (9)$$

The simulation time in both cases was recorded and the relative was calculated and listed in Table 6. The predicted value from eq. (6) in section 3 was also calculated and tabulated. The computational burden reduction ranges from 75 to 65 %. The predicted and recorded values from the simulation agree well. The small difference between them can be due to other operations that don't scale well with N^3.

5. Conclusion

Within the NEGF framework, a computationally efficient and accurate model was proposed. The approach was termed PCMS due to the separate coupling between even modes and odd modes. The PCMS was applied to nanoscale n-FinFETs and benchmarked against the full-coupling approach (CMS). The benchmarking was carried out on set of devices from the ITRS targets. In contrast to the fully UMS, the proposed approach is valid for both thin and thick Si film thickness. Excellent PCMS accuracy relative to the CMS with 65 to 75% reduction in simulation time was achieved. The PCMS is limited for symmetric structures and symmetric gates voltage. The proposed approach can be applied to other symmetric nanoscale devices like nano-wires, CNT and 3-D multi-gate transistors where even and odd transverse modes exist.

References

1. Singh N., F. Y. Lim, W. W. Fang, *et al.,* IEDM Tech. Dig., 2006, pp 547-550.
2. International Technology Roadmap for Semiconductor (ITRS) [online]. Available: "http://www.itrs.net".
3. Supriyo Datta, *Electronic Transport in Mesoscopic Systems,* Cambridge University Press, Cambridge, UK, 1995.
4. Datta S., *Nanoscale Device Modeling: the Green's Function Method*, Superlattices Microstruct. 2000, 28: 253.
5. Yasser M. Sabry, Tarek M. Abdolkader and Wael F. Farouk, Simulation of quantum transport in double-gate MOSFETs using the non-equilibrium Green's function formalism in real-space: A comparison of four methods, *Int. J. Numer. Model.*, 2010.
6. Khan H., V. Mamaluy, V. Vasileska, Ballistic Quantum-Mechanical Simulation of 10nm FinFET Using CBR Method, *J. Phys. Conf.*, Ser. 38 (2006) 196–199.
7. Venugopal R., Z. Ren, S. Datta, M. S. Lundstrom, D. Jovanovic, Simulating quantum transport in nanoscale transistors: real versus mode-space approaches, *Journal of Applied Physics*, 92 (7) (2002) 3730–3739.
8. Luisier M., A. Schenk, W. Fichtner, Quantum transport in two- and three- dimensional nanoscale transistors: coupled mode effects in the nonequilibrium Green's function formalism, *Journal of Applied Physics*, 100 (4) (2006) 043713.

9. Kurniawan O., P. Bai, E. Li, Ballistic calculation of nonequilibrium Green function in nanoscale devices using finite element method, *Journal of Physics D: Applied Physics*, 42 (2009) 105109.
10. Ren Z., R. Venugopal, S. Goasguen, S. Datta, and M. S. Lundstrom, nanoMOS 2.5: A Two-dimensional simulator for quantum transport in Double-gate MOSFETs, *IEEE Trans. Electron Devices*, vol. 50, Sep. 2003, pp. 1914–1925.
11. Yasser M. Sabry, Tarek M. Abdolkader and Wael F. Farouk, Uncoupled mode-space simulation validity for double gate MOSFETs, *ICM conference*, 2007; 351–354.
12. Wang J., E. Polizzi, and M. S. Lundstrom, A Three-Dimensional Quantum Simulation of Silicon Nanowire Transistors with the Effective Mass Approximation, *J. Appl. Phys.*, 96, 2192, 2004.
13. Oka Kurniawan, Man-Fai Ng, Wee Shing Koh, ZuanYi Leong, Erping Li, Simplified model for ballistic current–voltage characteristic in cylindrical nanowires, *Microelectronics Journal*, 41 (2010) 155–161.
14. Fiori G., G. Iannaccone and G. Klimeck, Coupled Mode Space Approach for the Simulation of Realistic Carbon Nanotube Field-Effect Transistors, *IEEE TRANSACTIONS ON NANOTECHNOLOGY*, VOL. 6, NO. 4, JULY 2007.
15. Negulescu C., N. Ben Abdallah, M. Mouis, An accelerated algorithm for 2D simulations of the quantum ballistic transport in nanoscale MOSFETs, *Journal of Computational Physics*, 225 (2007), no. 1, 74-99.
16. Alan Paussa, Francesco Conzatti, Dimitri Breda, Rossana Vermiglio, David Esseni and Pierpaolo Palestri, Pseudospectral Methods for the Efficient Simulation of Quantization Effects in Nanoscale MOS Transistors, *IEEE TRANSACTIONS ON ELECTRON DEVICES*, VOL. 57, NO. 12, DECEMBER 2010.
17. Tom J. Kazmierski, Dafeng Zhou, Bashir M. Al-Hashimi, and Peter Ashburn, Numerically Efficient Modeling of CNT Transistors With Ballistic and Nonballistic Effects for Circuit simulation, *IEEE TRANSACTIONS ON NANOTECHNOLOGY,* VOL. 9, NO. 1, JANUARY 2010 99.
18. Mohsen Hayati, Abbas Rezaei, Majid Seifi, CNT-MOSFET modeling based on artificial neural network: Application to simulation of nanoscale circuits, *Solid-State Electronics*, 54 (2010) 52–57.
19. Ramesh R., M. Madheswaran, K. Kannan, 3-D numerical modeling and simulation of nanoscale FinFET for the application in ULSI circuits, *Physica E*, 44 (2011) 80–86.
20. R. Ramesh, M. Madheswaran, K. Kannan, Self-consistent 3-D numerical modeling of a uniformly doped nanoscale FinFET using interpolating wavelets, *J Comput Electron*, (2011) 10:331–340.
21. Aryan Afzalian, Computationally efficient self-consistent born approximation treatments of phonon scattering for coupled-mode space non-equilibrium Green's Function, *JOURNAL OF APPLIED PHYSICS*, 110, 094517 (2011).
22. T. Abdolkader, W. Farouk, O. Omar and M. Hassan. FETMOSS: software tool for 2D simulation of double-gate MOSFET, *Int. J. Numer. Model*, vol.19, pp. 301-214, 2006.
23. Leland Chang, Peter Yu, Ballistic Transport in Silicon MOSFET's, *Physics 250 Term Paper,* May 2000 [online]. Available:http://hkn.eecs.berkeley.edu/~leland/coursework/phys250.pdf
24. El-Banna M.M., Y.M. Sabry, W. Fikry, O.A. Omar, Partial-Coupled Mode Space for quantum transport simulation in nanoscale double-gate MOSFETs, *International Conference on Microelectronics (ICM), 2010,* Page(s): 303 – 306, 2010.
25. Ferry D. and S. Goodnick, *Transport in Nanostructures*, Cambridge University Press, Cambridge, UK, 1997.
26. Ren Z., *Nanoscale MOSFETs: physics, simulation and design,* Ph.D. Dissertation, Purdue University, West Lafayette, October 2001.
27. Pierret R., *Advanced Semiconductor Fundamental*, Prentice Hall, 2003.
28. Colinge J. P., *FinFETs and other Multi-Gate Transistors*, Springer, 2007.
29. Carter T. A., R. A. Tapia & A. Papakonstantinou: *Linear Algebra, An Introduction to Linear Algebra for Pre-Calculus Students*, Rice University, May 1995 [online]. Available: http://ceee.rice.edu/publications.html.

2/20/2013